Progress In Electromagnetics Research M, Vol. 20, 179–190, 2011

NEAR FIELD FOCUSING EFFECT AND HYPERBOLIC DISPERSION IN DIELECTRIC PHOTONIC CRYSTALS

N. Yogesh and V. Subramanian*

Microwave Laboratory, Department of Physics, Indian Institute of Technology Madras, Chennai 600036, India

Abstract—This paper investigates the near field focusing behavior corresponding to the hyperbolic dispersion regime at the second band of the square lattice photonic crystal (PC). Numerical studies reveal the influence of the corner part negative refraction in the observed focusing effect, though the major part of the refraction is divergent at this hyperbolic regime. It is further observed that the investigated dispersion shows the surface mode behavior when the effective index of the PC slab is higher than the air medium. This aspect may be implemented for the excitation and transfer of near fields for an evanescent wave microscopy.

1. OBJECTIVE OF THE PROBLEM

The concept of flat lens focusing proposed by Veselago [1], Silin [2], and Pendry [3] can be realized from three possible electromagnetic media. Namely, the metamaterial [4, 5], photonic crystal [6], and an indefinite medium (whose permittivity and permeability tensors do not have same sign) [7–10]. The mechanism of flat lens imaging is accounted from negative refraction, in which a flat slab can be able to focus near fields with sub-wavelength features.

However, for a photonic crystal, the concept of flat lens imaging is not only addressed from negative refraction [11] but also from other approaches such as an anisotropic effect [12], partial band gaps [13–15], diffractive effects [16], the role of reflection [17], the effect of channeling from self-collimation [18, 19] and on the existence of surface modes [20] etc..

With respect to the existing approaches, this work attempts to understand the near field focusing behavior (Figure 1) at the operating

Received 7 July 2011, Accepted 25 August 2011, Scheduled 1 September 2011

* Corresponding author: Venkatachalam Subramanian (manianvs@iitm.ac.in).

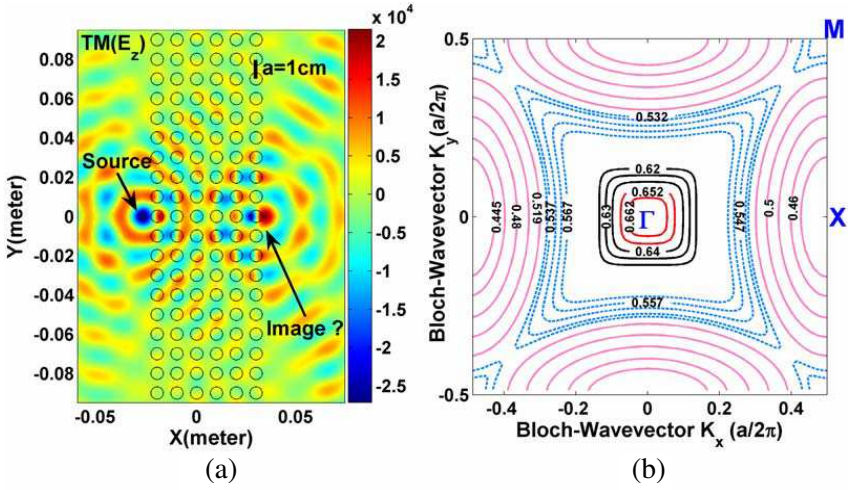

Figure 1. (a) The E_z field pattern at 16.45 GHz for a point source placed at $0.437a$ ('a' is the lattice constant taken to be 1 cm) behind the left side of the PC slab. (b) The plot of selected EFCs corresponds to the second band of the TM mode. Γ, X and M are the highest symmetry points of the irreducible Brillouin zone of the square lattice.

frequency (II band) corresponding to the hyperbolic dispersion regime of the square lattice PC. In general, the refraction solutions for any hyperbolic dispersion may show either the negative refraction of the power accompanied by the acute phase (Type-I) or the positive refraction of the power accompanied by the obtuse phase (Type-II) [21]. In case, if a medium holds Type-I refraction, it is possible to design a flat lens with sub-wavelength features that will show the partial focusing effect [22]. On the other hand, if a medium possesses Type-II refraction, then the flat slab will show the divergence effect for a point source placed near to it.

It is noted that the investigated dispersion regime (dashed curves in Figure 1(b)) belongs to the Type-II refraction. However, their edges are closed and it has a convex nature due to the effect of band folding and periodicity. Suppose, an electromagnetic ray hits the corner of such a dispersion regime, it may result in negative power bending owing to their convex curvature. The objective of this paper is to verify whether such corner part refraction is responsible for the observed focusing effect shown in Figure 1(a).

It is important to note that the corner part of the hyperbolic dispersion regime is accessible, only when the effective index of the

PC slab is smaller than the index of the air medium. In other words, the air Eigen Frequency Contour (EFC) should be larger than the PC EFC. For the case of higher effective index PC slab, where the PC EFC is intersecting with the air EFC, the strong surface modes existing on the either side of the PC slab are observed.

2. MECHANISM OF FOCUSING

2.1. Ray Tracing

The analysis is made with the square lattice PC consists of periodic arrangement of dielectric circular rods in an air background. The normalized radius and the relative dielectric permittivity of the circular rods are $\tilde{r} = 0.313a$ ('a' is the lattice constant), and $\varepsilon_r = 3.6$ respectively. Figure 1(a) shows the E_z field pattern at 16.45 GHz for a point source placed at $0.437a$ from the left side of the PC slab. This field computation is performed with the Finite-element methodology (FEM) based e-m solver FEMLAB [23]. The point source is excited with the Transverse Magnetic (TM) polarization, where the electric field vector is along the length of the dielectric pillars. To understand the imaging mechanism, the wave-vector diagram given in Figure 1(b) is obtained with plane wave methodology based free e-m solver MPB [24]. It shows the selective Eigen Frequency Contours (EFCs) for the second band of the TM mode.

As a first principle, the ray tracing analysis is performed on these hyperbolic dispersion contours (blue-dashed lines). The necessary information required for the ray tracing are the band slope and EFC's curvature. It is evident from Figure 1(b) that for increase in frequencies, the hyperbolic curves are shrinking towards the Γ point of the Brillouin zone. Moreover, the band slope is negative at this frequency regime. This suggests the inward normal gradient for the group ($\vec{V}_g = \frac{\partial \omega}{\partial k}$) velocity vectors.

These details are incorporated in the repeated Brillouin zone scheme given in Figure 2. The imaging frequency of 16.45 GHz is taken for the ray tracing and the corresponding PC EFCs and air are drawn (normalized angular frequency is $0.548(2\pi c/a)$, where 'a' is the lattice constant). The selected frequency is common to both TM2 and TM3 bands and it has hyperbolic shapes at Γ and M point respectively. Since the air EFC is larger than the PC EFC (effective index of the PC slab is lesser than the air medium), the incident ray at all angles would not couple to the PC slab and it will be totally reflected because of the non-availability of the PC contour.

For the first case, the ray at smaller incident angle is taken as

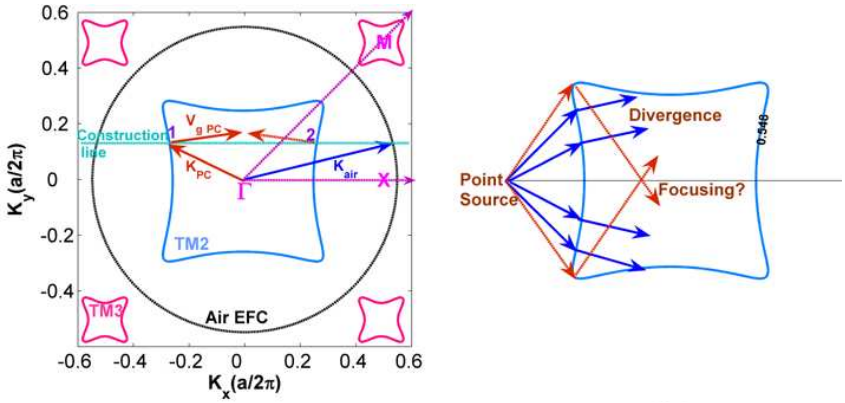

Figure 2. (a) Ray tracing at the normalized angular frequency of $0.548(2\pi c/a)$. K_{air} denotes the incident wavevector direction. V_{gPC} and K_{PC} are the power and phase refracted components of the PC slab. (b) Refraction picture for the point source. Solid blue rays show the divergence, whereas the red rays show the focusing.

shown in Figure 2(a). The construction line intersects the PC EFC at the points 1 and 2. In solution 2, the group velocity component is pointing towards the incident radiation direction and hence it is omitted from the analysis. On the other hand, the solution 1 gives the regular refracted signal, in which the phase (k_{PC}) and power (V_{GPC}) refracted components are indicated with the solid red lines in Figure 2(a). It is clear that at smaller incident angle, the refraction is positive and subsequently, one can see the divergence effect for a point source for almost all incident angles as shown with solid blue lines in Figure 2(b).

In case, if the incident ray meets the corner of the dispersion contour, it may result in negative refraction as per the red solid line given in Figure 2(b). Since the corner part has a convex nature, one may expect the focusing effect solely from the corner as shown in Figure 2(b).

2.2. Scattering Parameter

To reveal the response of the hyperbolic dispersion regime for various incident angles, the scattering parameter such as the transmission (T) and reflection (R) is computed for the observed frequency using Transfer Matrix Methodology (TMM) based free e-m solver

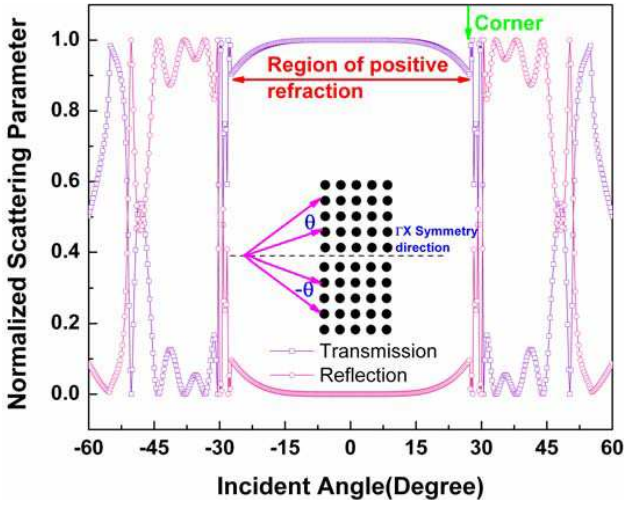

Figure 3. Normalized scattering parameter for the eight-layer PC slab oriented along ΓX symmetry direction at $\omega = 0.548(\frac{2\pi c}{a})$.

Translight [25]. The eight-layer PC slab is taken for the computation of normalized scattering parameters and the wave propagation along ΓX symmetry direction is considered. The incident angle of the e-m ray is varied from $-60°$ to $60°$ and the results are plotted in Figure 3.

Similar to the ray tracing analysis, the scattering plot clearly shows the three different scattering regime of the hyperbolic dispersion at $\omega = 0.548(\frac{2\pi c}{a})$. The first regime spanning from $-27°$ to $27°$ shows the smooth variation in the T curve, where the transmission is nearly maximum. This regime is corresponding to the divergence part of the dispersion contour. The second regime spanning within the $27°$ to $30°$ shows sudden fall and rise in the T and R curve, as this may correspond to the corner part of the dispersion regime. Any incident angle greater than the $30°$ is not coupled to the PC slab, as this would result in total reflection (R is maximum and T is minimum) and hence further propagation along ΓX symmetry direction is forbidden, because of the non-availability of the PC contour (partial band gaps).

2.3. Refraction

In order to verify the above result, the refraction behavior of this hyperbolic dispersion regime is studied using FDTD methodology based free e-m solver F2P [26]. The continuous Gaussian line source of size $20a$, ('a' is the lattice constant) at normalized frequency of

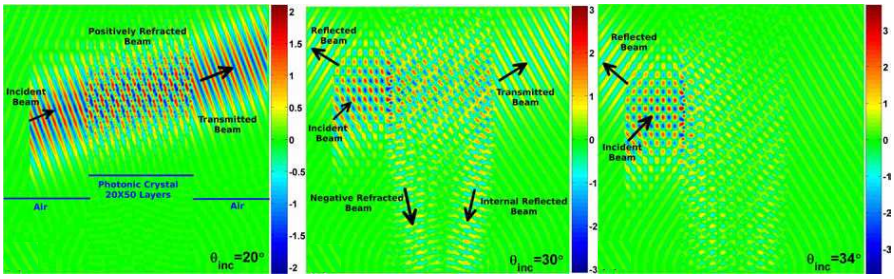

(a) (b) (c)

Figure 4. (a)–(c) The E_z field pattern recorded at 10000 time steps for a Gaussian pulse of size $20a$ at normalized frequency of $0.548(2\pi c/a)$ is impinged on 20×50-layer PC slab.

$\omega = 0.548(\frac{2\pi c}{a})$ is impinged on a 20×50-layer PC slab. Perfectly matched boundary condition is employed around the computational domain. The monitored E_z fields at 10000 time steps are plotted in Figure 4. When an incident angle is 20°, one would clearly see the positive refraction of the beam inside the PC slab in Figure 4(a). Moreover, the refraction is essentially the single beam and one can see the maximum transmission in the output interface.

The corner angle (the incident angle at which the light meets the corner of the hyperbolic dispersion contour) behavior is shown in Figure 4(b). Since the construction line intersects the corner of the dispersion regime at several points, the refraction involves multiple beams including the negative refractive components and an internal reflected ray. It may be noted that the major refracted component involves mixed refraction, as one cannot able to separate the phase and power propagation directions. In Figure 4(c), one can see the near total reflection, when the incident angle is greater than the corner angle. It is clear that the corner part of the dispersion regime is the only portion showing the negative power bending among the entire dispersion regime.

2.4. Formation and Evolution of Image's Spot Size

To clarify about the formation of image, metal slit (made of Perfect Electric Conductor-PEC) is placed in between the PC slab and the point source as shown in Figure 5(a). By adjusting the slit's separation, one can able to select/block the higher incident angle rays emitted by the point source. This effect of slit width on the image formation is studied through FEMLAB and it is given in Figure 5.

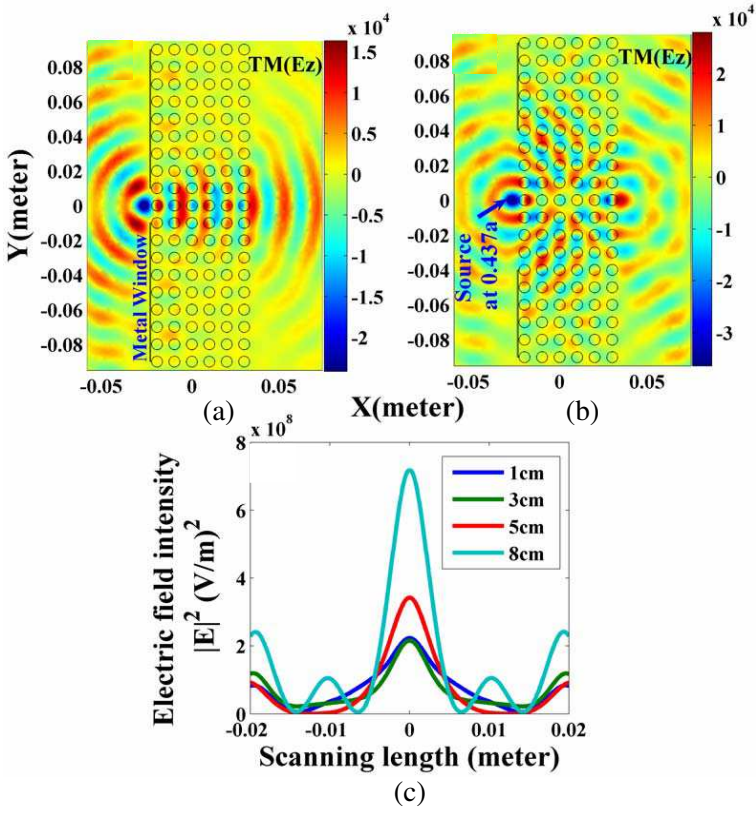

Figure 5. (a) The separation of divergence by metal slit. (b) The recovery of focusing at the largest separation of the metal slit. In both the cases the source is placed at $0.437a$ ('a' is the lattice constant taken to be 1 cm) and the field pattern is shown for 16.45 GHz. (c) The plot of electric field intensity scanned at the image plane for various slit's separations.

When the slit's separation is small, say, about 2 cm (Figure 5(a)), one would see the divergence behavior as shown in Figure 5(a). It is clear that the dispersion regime will show only the divergence effect for lower angle incident rays. (In case, if the flat lens is based on all angle negative refraction, then the PC slab will show the imaging effect even for a small slit source [27].). On the other hand, if the slit separation is very large, all sort of incident angles are impinged on the PC slab and one would clearly see the well-defined image spot as in Figure 5(b). In between these two extremes, one can see the evolution of imaging in

Figure 5(c). It is evident that the variation in the slit separation results in complete divergence (1 and 3 cm) to well-defined converged spot size (upon opening of slit). This simple real space demonstration provides the one possible evident for the role of corner part of the dispersion regime in the focusing effect.

Some of the observed characteristics of this focusing effect are listed as follows;

1. It is found that the focused spot size is within the sub-wavelength dimensions. For example, the computed Full-width at Half-Maximum (FWHM) value of the image spot observed in Figure 5(b) is of the order of 0.2972λ, where 'λ' is the operating wavelength (1.8237 cm).
2. Focusing is observed only when the source is placed along the highest symmetry point (Γ) of the square lattice PC slab. Any asymmetry in the source's position (away from Γ point) result in phase mismatching, as the incident rays will not hit the corner at the same time and result in the absence of imaging. This aspect of asymmetry of source's position in imaging mechanism can also be found for the case of quasi-symmetric PC slab [28].
3. Since the PC slab operated at this hyperbolic dispersion regime is inhomogeneous and anisotropic, the variation in the photonic layers does not the show the unique focusing behavior.

3. SURFACE MODES

Other than the corner-part focusing effect, the existence of surface modes [29] is observed for a range of hyperbolic dispersion frequencies corresponding to the higher-effective index PC system. For example, the case of direct PC consists of Germanium ($\varepsilon_r = 18.0$) rods arranged in air medium is given in Figure 6 (The normalized radius and the periodicity are the same as that of Figure 1(a)). Though the wave-vector diagram does not describe the formation of surface modes, it is useful to mention that for a higher-effective index PC slab, the range of hyperbolic dispersion contours are intersecting with the air EFC. This is shown in Figure 6(a), where the PC EFC at 8.49 GHz is intersecting with the corresponding air EFC.

When a point source is excited near to the PC slab (7×37 layers) at this frequency (8.49 GHz), the fields are confined to the either side of the PC slab as shown in Figure 6(b). The electric field profile scanned along the surface of the PC slab in the object and image plane are plotted in Figure 6(c). It is evident that the PC slab operated at this frequency regime effectively transfers the near fields. Owing

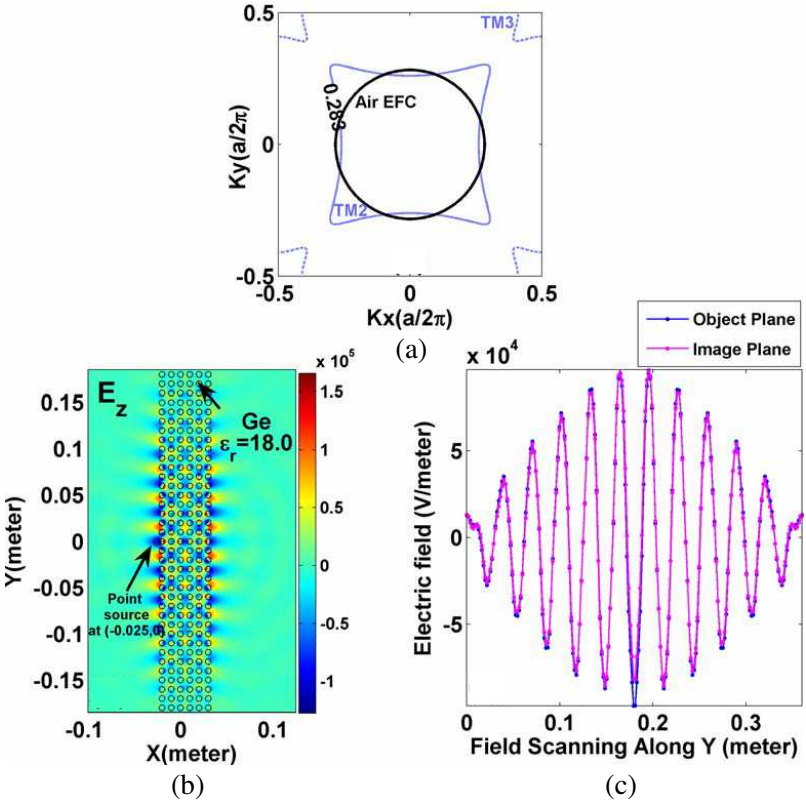

Figure 6. (a) PC and air EFCs corresponding to the Ge direct PC at normalized angular frequency of $0.283(2\pi c/a)$. (b) E_z field pattern at 8.49 GHz for a PC slab consists of Ge rods (normalized radius $0.313a$, 'a' is the lattice constant taken to be 1 cm). The point source is placed at $0.187a$ $(-0.025, 0)$ from left side of the PC slab. (c) The scanned E-field patterns corresponding to the object and image plane of the Ge PC slab.

to the utility of evanescent fields, one can implement this surface mode behavior for Scanning-near-field-microwave-microscopy (SNMM) technique, where the PC slab at this hyperbolic dispersion regime can serve as the near field exciter/collector.

4. CONCLUSIONS

The near field focusing effect arising from the hyperbolic dispersion of the dielectric photonic crystal is reported in this work. The ray tracing analysis, scattering parameter and refraction studies reveal the anisotropic nature of the dispersion regime, where various parts of the dispersion shows different type of refraction nature. It is found that except at the corner of the dispersion regime, the refraction is divergent for all incident angles. The corner part shows the multi-refringence behavior including the negative refractive component and higher order reflected ray. It is numerically verified that the corner part is the only portion showing the negative power bending and it would be the possible origin for the observed focusing effect. It is noted that the corner part is the consequence of the periodicity and it can be modulated by the dielectric/magnetic strength of the periodic system. Moreover, such a convex regime is accessible only when the effective index of the PC slab is lesser than the air medium.

For the second case, the surface modes arising from the hyperbolic dispersion of the PC slab consists of high dielectric constituents are reported. Though presented dielectric dispersion is inhomogeneous and anisotropic, these surface modes behavior can be employed for on-chip image transfer and microwave-microscopy etc..

REFERENCES

1. Veselago, V. G., "The electrodynamics of substances with simultaneously negative values of ε and μ," *Sov. Phys. Usp.*, Vol. 10, 509–514, 1968.
2. Silin, R. A., "Possibility of creating plane-parallel lenses," *Opt. Spectrosc.*, Vol. 44, 109, 1978.
3. Pendry, J. B., "Negative refraction makes a perfect lens," *Phys. Rev. Lett.*, Vol. 85, 3966, 2000.
4. Ramakrishna, S. A. and T. M. Grezegorczyk, *Physics and Applications of Negative Refractive Index Materials*, 77–143, CRC Press, Boca Raton, 2009.
5. Cheng, Q., H.-F. Ma, and T.-J. Cui, "A complementary lens based on broadband metamaterials," *Journal of Electromagnetic Waves and Applications*, Vol. 24, No. 1, 93–101, 2010.
6. Joannopoulos, J. D., S. G. Johnson, J. N. Winn, and R. D. Meade, *Photonic Crystals Molding the Flow of Light*, 2nd Edition, Princeton University Press, Princeton, New Jersey, 2008.

7. Smith, D. R. and D. Schurig, "Electromagnetic wave propagation in media with indefinite permittivity and permeability tensors," *Phys. Rev. Lett.*, Vol. 90, No. 7, 077405, 2003.
8. Smith, D. R., P. Kolinko, and D. Schurig, "Negative refraction in indefinite media," *J. Opt. Soc. Am. B*, Vol. 21, No. 5, 1032–1043, 2004.
9. Qiao, S., G. Zheng, H. Zhang, and L.-X. Ran, "Transition behavior of k-surface: From hyperbola to ellipse," *Progress In Electromagnetics Research*, Vol. 81, 267–277, 2008.
10. Kong, F., B.-I. Wu, H. Hunag, J. Huangfu, S. Xi, and J. A. Kong, "Lateral displacement of an electromagnetic beam reflected from a grounded indefinite uniaxial slab," *Progress In Electromagnetics Research*, Vol. 82, 351–366, 2008.
11. Notomi, M., "Theory of light propagation in strongly modulated photonic crystals: Refractionlike behavior in the vicinity of the photonic band gap," *Phys. Rev. B*, Vol. 62, No. 16, 10696–10705, 2000.
12. Luo. C., S. G. Johnson, J. D. Joannopoulos, and J. B. Pendry, "All-angle negative refraction without negative effective index," *Phys. Rev. B*, Vol. 65, 201104(R), 2002.
13. Fang, Y. and T. Shen, "Diverse imaging of photonic crystal be the effects of channeling and partial band gap," *Optik*, Vol. 118, 100–102, 2007.
14. Sun, G. and A. G. Kirk, "Analyses of negative refraction in the partial bandgap of photonic crystals," *Opt. Express*, Vol. 16, No. 6, 4330–4336, 2008.
15. Tang, Z., R. Peng, Y. Ye, C. Zhao, D. Fan, H. Zhang, and S. Wen, "Optical properties of a square-lattice photonic crystal within the partial band gap," *J. Opt. Am. A*, Vol. 24, No. 2, 379–384, 2007.
16. Minin, I. V., O. V. Minin, Y. R. Triandaphilov, and V. V. Kotlyar, "Subwavelength diffractive photonic crystal lens," *Progress In Electromagnetics Research B*, Vol. 7, 257–264, 2008.
17. Fang, Y.-T. and H.-J. Sun, "Imaging by photonic crystal using reflection and negative refraction," *Chin. Phys. Lett.*, Vol. 22, No. 10, 2674–2676, 2005.
18. Li, Z.-Y. and L.-L. Lin, "Evaluation of lensing in photonic crystal slabs exhibiting negative refraction," *Phys. Rev. B*, Vol. 68, 245110, 2003.
19. Feng, S., L. Ao, and Y.-Q. Wang, "Engineering the near-field imaging of a rectangular-lattice photonic-crystal slab in the second band," *Science in China Series G: Physics, Mechanics and*

Astronomy, Vol. 52, No. 1, 87–91, 2009.

20. Luo, C., S. G. Johnson, J. D. Joannopoulos, and J. B. Pendry, "Subwavelength imaging in photonic crystals," *Phys. Rev. B*, Vol. 68, 045115, 2003.
21. Wang, M.-Y., J. Xu, J. Wu, B. Wei, H.-L. Li, T. Xu, and D.-B. Ge, "FDTD study on wave propagation in layered structures with biaxial anisotropic metamaterials," *Progress In Electromagnetics Research*, Vol. 81, 253–265, 2008.
22. Smith, D. R., D. Schurig, J. J. Mock, P. Kolinko, and P. Rye, "Partial focusing of radiation by a slab of indefinite media," *Appl. Phys. Lett.*, Vol. 84, No. 13, 2244–2246, 2004.
23. Whiteman, J. R., *The Mathematics of Finite Elements and Applications*, John Wiley and Sons, Chichester, 1998. http://www.comsol.com.
24. Johnson, S. G. and J. D. Joannopoulos, "Block-iterative frequency-domain methods for Maxwell's equations in a plane wave basis," *Opt. Express*, Vol. 8, No. 13, 173–190, 2001. http://ab-initio.mit.edu/mpb.
25. Reynolds, A. L., "Translight software," The University of Glasgow, 2000. Email id: areynolds@elec.gla.ac.uk.
26. Qiu, M., *F2P: Finite-difference Time-domain 2D Simulator for Photonic Devices*, http://www.imit.kth.se/info/FOFU/PC/F2P.
27. Lu, Z., J. A. Murakowski, C. A. Schuetz, S. Shi, G. J. Schneider, and D. W. Prather, "Three-dimensional subwavelength imaging by a photonic-crystal flat lens using negative refraction at microwave frequencies," *Phys. Rev. Lett.*, Vol. 95, 153901, 2005.
28. Zhang, X., Z. Li, B. Cheng, and D.-Z. Zhang, "Non-near-field focus and imaging of an unpolarized electromagnetic wave through high-symmetry quasicrystals," *Opt. Express*, Vol. 15, No. 13, 1292–1300, 2007.
29. Entezar, S. R., A. Namdar, H. Rahimi, and H. Tajalli, "Localized waves at the surface of a single-negative periodic multilayer structure," *Journal of Electromagnetic Waves and Applications*, Vol. 23, No. 2–3, 171–182, 2009.